Investigating temperature degradation in THz quantum cascade lasers by examination of temperature dependence of output power

Asaf Albo[a] and Qing Hu
Department of Electrical Engineering and Computer Science and Research Laboratory of Electronics, Massachusetts Institute of Technology, Cambridge, Massachusetts 02139, USA

(Received 4 March 2015; accepted 25 March 2015; published online 2 April 2015)

In this paper, we demonstrate a method to investigate the temperature degradation of THz quantum cascade lasers (QCLs) based on analyzing the dependence of lasing output power on temperature. The output power is suggested to decrease exponentially with some characteristic activation energy indicative of the degradation mechanism. As a proof of concept, Arrhenius plots of power versus temperature are used to extract the activation energy in vertical transition THz QCLs. The extracted energies are consistent with thermally activated longitudinal optical-phonon scattering being the dominant degradation mechanism, as is generally accepted. The extracted activation energy values are shown to be in good agreement with the values predicted from laser spectra. © *2015 AIP Publishing LLC*. [http://dx.doi.org/10.1063/1.4916961]

Semiconductor laser performance versus temperature is frequently characterized by examining the threshold current evolution according to a phenomenological relationship $J_{th} = J_1 + \exp(T/T_0)$, where T_0 is an experimentally determined parameter. Unfortunately, there is no straightforward way to relate T_0 to the underlying physics of the temperature degradation. This paper suggests an alternative characterization of semiconductor lasers based on the evolution of maximum lasing output power versus temperature. The method is validated through examining the temperature degradation of vertical transition terahertz quantum cascade lasers (THz-QCLs), where thermally activated LO phonon scattering (Fig. 1(a)) is widely believed to be the dominating mechanism.

The output power of a semiconductor laser is given by[1]

$$P_{out} = \frac{1}{2}\frac{h\upsilon}{e}\frac{\alpha_m}{\alpha_m + \alpha_w} A\eta_i (J - J_{th}),$$

where P_{out} is the output power, $h\upsilon$ is the photon energy, $A = L \times W$ the contact area, e the electron charge, α_m is the mirror loss, α_w is the waveguide loss, J and J_{th} are the injected current density and threshold current density, respectively, and η_i is the internal quantum efficiency. The current density due to stimulated emission is related to the injected current and threshold current densities by $J_{st} = \frac{\eta_i}{N_{mod}}(J - J_{th})$, and can be approximated by

$$J_{st} \approx \frac{e\Delta n_{th}}{\tau_{st}},$$

where $\Delta n_{th} = \frac{g_{th}}{\sigma_g} L_{mod}$ is the 2D clamped population inversion at the lasing threshold g_{th} determined by the lasing condition (balance of gain and loss). σ_g is the gain cross section, L_{mod} is the QCL period (module) thickness, N_{mod} is the number of modules, and $\frac{1}{\tau_{st}}$ is the stimulated emission rate. Therefore,

$$P_{out} = \frac{1}{2}\frac{h\upsilon}{e}\frac{\alpha_m}{\alpha_m + \alpha_w} AN_{mod} J_{st} \approx \frac{1}{2} h\upsilon \frac{\alpha_m}{\alpha_m + \alpha_w} AN_{mod}\frac{\Delta n_{th}}{\tau_{st}}.$$

Assuming that mirror and waveguide losses are temperature independent, then the clamped population inversion, Δn_{th}, is also temperature independent. Any temperature dependence of P_{out} must, therefore, be due to the stimulated emission rate, $\frac{1}{\tau_{st}}$.

To analyze $\frac{1}{\tau_{st}}$, for simplicity we focus on the case of a three-subband THz QCL (see Figure 1(b)). Neglecting back-filling effects, the stimulated emission rate can be shown to be[2]

$$\frac{1}{\tau_{st}} = \sigma_g S = \frac{\frac{1}{\tau_{21}}\left(2 + \frac{\tau_{13}^*}{\tau_{31}}\right) + \frac{1}{\tau_{32}}\left(1 + \frac{\tau_{13}^*}{\tau_{21}}\right)}{\left(2 + \frac{\tau_{13}^*}{\tau_{21}}\right) + \left(1 + \frac{\tau_{13}^*}{\tau_{31}}\right)} \times \left[\frac{\Delta n_{ul}(S=0)}{\Delta n_{th}} - 1\right], \quad (1)$$

where τ_{13}^* is the injector ($1'$) to the upper lasing level (3) tunneling time, τ_{31} is the LO-phonon scattering time from the upper lasing level (3) to the injector level of the next module (1), τ_{21} is the LO-phonon scattering time from the lower lasing level (2) to the injector level of the next module (1), τ_{32} is the LO-phonon scattering time from the upper lasing level (3) to the lower lasing level (2), S is the photon flux in the cavity, and $\Delta n_{ul}(S=0)$ is the non-lasing population inversion that is given by the solution of the rate equation set below threshold ($\tau_{st} = \infty$)[2]

$$\Delta n_{ul}(S=0) = n_3 - n_2 = n\frac{\frac{1}{\tau_{13}^*}\left(1 - \frac{\tau_{21}}{\tau_{32}}\right)}{\frac{1}{\tau_{13}^*}\left(2 + \frac{\tau_{21}}{\tau_{31}}\right) + \frac{1}{\tau_{31}} + \frac{1}{\tau_{32}}},$$

where n is the total electron population per QCL period.

Let us consider the normalized power $\frac{P_{out}(T)}{P_{out\,max}}$. In the absence of temperature induced mode-hopping (no changes to power collection, α_m, and $h\upsilon$), $\frac{P_{out}(T)}{P_{out\,max}} = \frac{S(T)}{S_{max}} = \frac{S(T)}{S(0)}$. A key observation is that the prefactor to the square brackets in Eq. (1) is slowly varying with temperature compared to the

[a]asafalbo@gmail.com

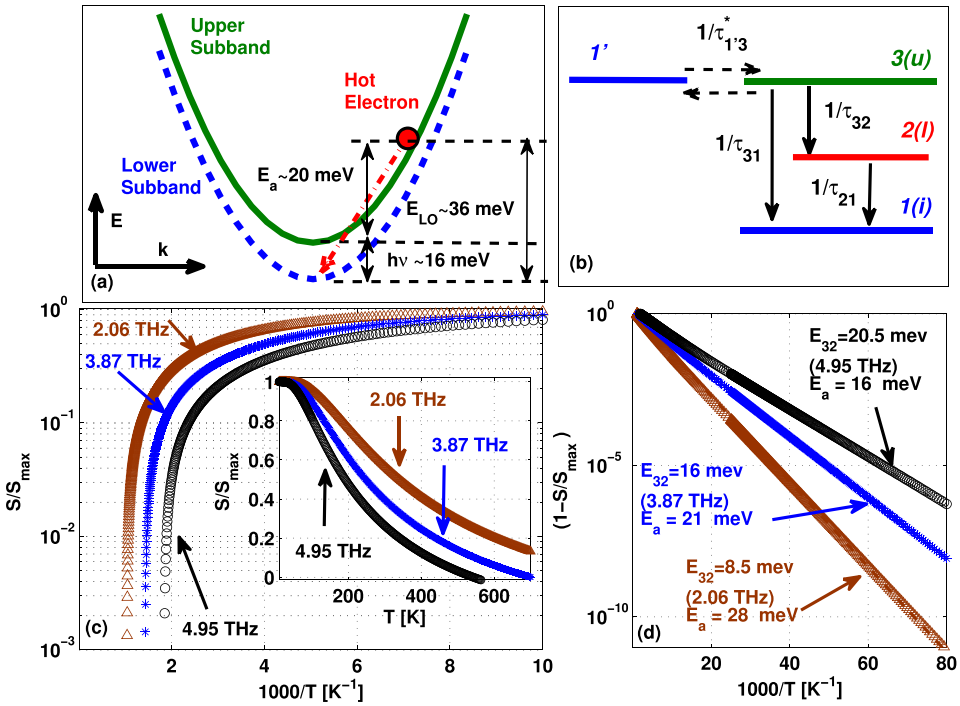

FIG. 1. (a) Illustration of thermally activated intersubband LO-phonon scattering process. (b) Schematic of a three-level THz-QCL. (c) Normalized photon flux (output power) as function of the inverse temperature in semi-logarithmic scale and in linear scale (inset). (d) A semi-logarithmic plot of $(1-\frac{S(T)}{S_{max}})$, where S is the calculated photon flux according to Eq. (1) and $\frac{P_{out}(T)}{P_{out\,max}} \approx \frac{S(T)}{S_{max}}$, with the fitted activation energy values. The calculations were conducted for three lasing frequencies of 8.5 meV (2.06 THz), 16 meV (3.87 THz), and 20.5 meV (4.95 THz). The parameters used for the calculation are $\tau_{21} = 0.2$ ps, $\tau_{31} = 4$ ps, $\tau^*_{13} = 1$ ps, $\tau_{32} = 0.2 \times e^{\frac{E_a}{kT}}$ ps, $n = 6\times10^{15}\,\mathrm{cm}^{-3}$, $g_{th} = 18\,\mathrm{cm}^{-1}$, $L_{mod} = 500$ Å, $f = 0.9$, and gain bandwidth of 1 THz.

variation of $\Delta n_{ul}(S=0)$ (to be computationally justified below). If we neglect the temperature dependence of the prefactor in Eq. (1), then clearly

$$\frac{P_{out}(T)}{P_{out\,max}} \approx \frac{\Delta n_{ul}(T) - \Delta n_{th}}{\Delta n_{ul}(0) - \Delta n_{th}}. \tag{2}$$

The normalized power is, therefore, a probe of the temperature dependence of the unclamped population inversion $\Delta n_{ul}(S=0)$. Although this result is derived for a three-level THz QCL, we make the ansatz that Eq. (2) holds in general.

The maximum operating temperature (T_{max}) reported so far for THz-QCLs based on GaAs/AlGaAs is ~200 K in pulsed operation.[3] A major cause of temperature degradation is posited to be thermally activated LO-phonon scattering[4,5] in which hot electrons in the upper lasing subband are sufficiently energetic to emit LO-phonons and relax nonradiatively to the lower lasing level (see Fig. 1(a)). Due to this, and other possible thermally activated processes, assume that the unclamped population deteriorates with some activation energy, E_a, according to the mathematical form $\Delta n_{ul}(T) = \Delta n_{ul}(0) - n_0 e^{\frac{-E_a}{kT}}$, where T is the upper-level electron temperature. The normalized output power therefore takes the form

$$\frac{P_{out}(T)}{P_{out\,max}} \approx \frac{\Delta n_{ul}(0) - n_0 e^{\frac{-E_a}{KT}} - \Delta n_{th}}{\Delta n_{ul}(0) - \Delta n_{th}} = 1 - a e^{\frac{-E_a}{kT}},$$

where $a = \frac{n_0}{\Delta n_{ul}(0) - \Delta n_{th}}$ is a constant. Then the slope of $\ln(1 - \frac{P_{out}(T)}{P_{out\,max}})$ versus inverse temperature (Arrhenius plot) yields the activation energy, E_a, which provides insight into what specific mechanism might be responsible for the temperature degradation.

To validate this method computationally, the power-temperature curves of a three-subband THz QCL are shown in Figures 1(c) and 1(d), calculated according to Eq. (1) without the approximation of Eq. (2). We assume an exponentially decreasing upper level lifetime due to thermally activated LO phonon scattering (model parameters are elaborated upon in the figure caption). The activation energies extracted from Figure 1(d) agree with the expected value of $\hbar\omega_{LO} - E_{32}$, where $\hbar\omega_{LO}$ is the LO phonon energy, and E_{32} is the lasing energy. (The T_{max} values predicted by the three-subband model are unrealistically high due to an oversimplified description of scattering. This is unimportant for the analysis in this paper, however.)

The validity of the above method can be shown alternatively by a more specific argument as follows. Under the reasonable assumption that $\tau_{31} \gg \tau_{32}$, it is straightforward (for example, based on the derivations on page 114 in Ref. 6) to obtain the relation,

$$P_{out} = \frac{\text{const}}{\tau_{32}} \times \left[J \times \frac{(\tau_{32} - \tau_{21})}{e} - (\alpha_m + \alpha_w) \times \frac{L_{mod}}{\sigma_g} - n_2^{therm} \right],$$

where n_2^{therm} is the thermal backfilling of the lower laser level; assumed to vary slowly with temperature in comparison to τ_{32}. Now the maximum power is obtained at maximum current J_{max}, which usually does not depend strongly on temperature. Furthermore, τ_{21} is dominated by optical phonon emission and should not depend much on temperature as long as the thermal energy $KT < E_{LO}$. Then, the output power is in the form of $P_{out} = c - \frac{d}{\tau_{32}}$ with c and d being constants. Thus, the Arrhenius plot for $1 - \frac{P_{out}(T)}{P_{out}(T=0)}$ probes the behavior of τ_{32}, which is proportional to $\exp(\frac{E_a}{kT})$ as both seen in the numerical calculations presented above and the experimental data presented later.

To validate this technique experimentally, we use it to analyze vertical transition THz QCLs. Vertical active region THz QCLs are particularly sensitive to thermally activated LO phonon scattering, due to their strong upper-level and

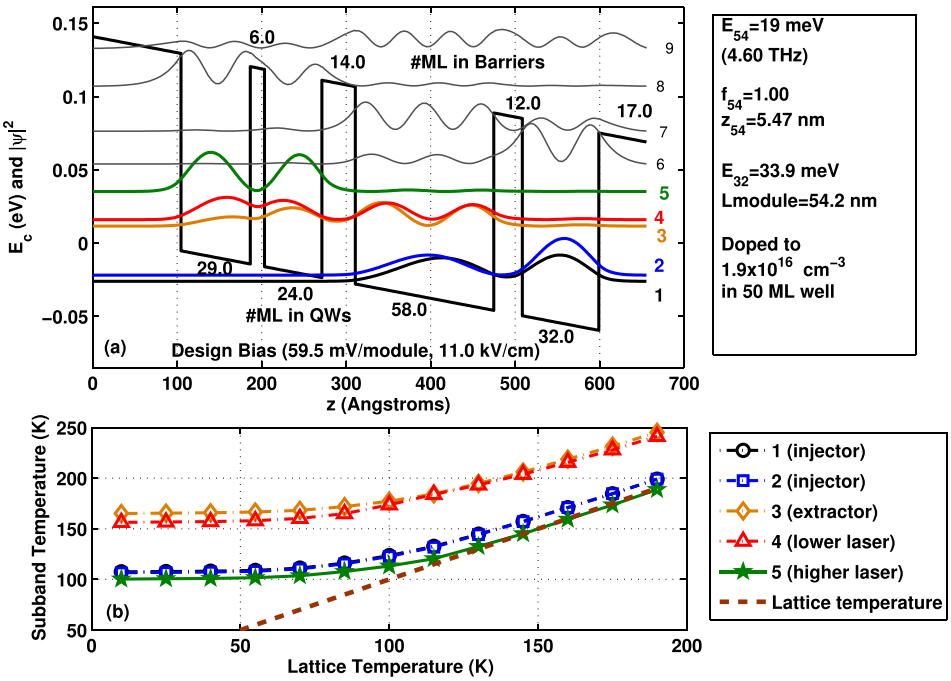

FIG. 2. (a) FL183R-2 band diagram, as an example of the FL structures. (b) Calculated electron subband temperatures at a bias of 10.9 kV/cm for the five principle subbands in (a) based on the formulas in Ref. 2.

lower-level wavefunction overlap in real-space. For this study, five resonant-phonon THz-QCLs were chosen for examination (two-well injector, two-well active region). A representative band structure scheme is shown in Figure 2(a). The samples vary in frequency from ~2 THz to ~5 THz. The details on layer sequences and waveguide type are summarized in Table I and elaborated upon in Ref. 7.

Equation (1) uses the electronic temperature of the upper-level subband, which may be hotter than the lattice. Unfortunately, the electronic temperature is not readily accessible in experiment, unlike the lattice temperature (which is well approximated by the heatsink temperature in pulsed operation). To investigate the relationship between electronic and lattice temperatures, subband temperatures are calculated based on methods used in Ref. 2. Figure 2(b) shows the calculated electron subband temperatures for the five principle subbands of the FL183R-2 structure in Figure 2(a). At low temperatures, there is significant electron heating due to the dominance of elastic scattering. However, as the lattice temperature rises, LO-phonon scattering becomes dominant, which efficiently cools the electrons down to lattice temperature. In the case of the upper laser level, below the lattice temperature of $T_L \sim 100$ K, the subband temperature is floored at about ~100 K and above which the electrons temperature converges to the lattice temperature. We conclude that significant electron heating occurs only at low temperatures, so it is reasonable to use the lattice temperature in place of the electronic temperature for analysis if we put emphasis on the high temperature data in our Arrhenius fit, with expectation that deviations will occur due to electron heating at low lattice temperatures.

The pulsed light-current (L-I) measurements at several temperatures and the spectral response are shown in Figures 3(a)–3(e). Hereafter, the samples are labeled by their lasing frequency and waveguide type (Table I and Figures 3(a)–3(e); for example, sample S22-MM is the sample which lases at 2.2 THz and clad in a metal-metal (MM) waveguide; similarly, a sample which was clad in a semi-insulating surface-Plasmon waveguide is labeled as SISP). As shown in Table II, the samples lase close to their designed lasing frequencies/energies. The L-I curves are approximately linear and parallel at different temperatures up to their measured maximum intensity, indicating a low degree of mode hopping.

The threshold current dependence on temperature and its related parameter T_0 are presented in Figure 4(a) and Table II, respectively. Figures 4(b) and 4(c) present the normalized peak power versus temperature in linear scale and versus the inverse temperature in semi-logarithmic scale (Arrhenius plot), respectively. A zoom-in of the latter on the first decade with a broader temperature range is shown in its inset. Figure 4(d) presents the Arrhenius plots $\ln(1 - \frac{P_{out}(T)}{P_{out\,max}}) \approx \ln(a) - \frac{E_a}{KT}$, as well as the extracted activation energies. The exponential character of the normalized power drop is clearly seen over a two-decade span in the higher T_{max}

TABLE I. The samples data. Additional details can be found in Ref. 7.

Name	Structure	Designed lasing energy [meV]	Designed oscillator strength	Expected activation energy [meV]	Layer sequence [#ML]	Process
S22-MM	FL175M-M3	9.9	0.81	26	**18**/29/**11**/24/**15**/57/**13**/33	MM (Cu-Cu), Wet etched
S27-MM	FL178C-M10	12.9	0.87	23	**16.9**/28.9/**9**/23.9/**15**/56.8/**13**/32.9	MM (Cu-Cu), Wet etched
S41-MM	FL183R-2	19	1	17	**17**/29/**6**/24/**14**/58/**12**/32	MM (Cu-Cu), Wet etched
S43-SISP	FL183R-2	19	1	17	**17**/29/**6**/24/**14**/58/**12**/32	SISP, Dry etched
S49-SISP	FL179R-M1	20.2	0.91	16	**19**/29/**5.5**/24/**15**/58/**13**/32	SISP, Dry etched

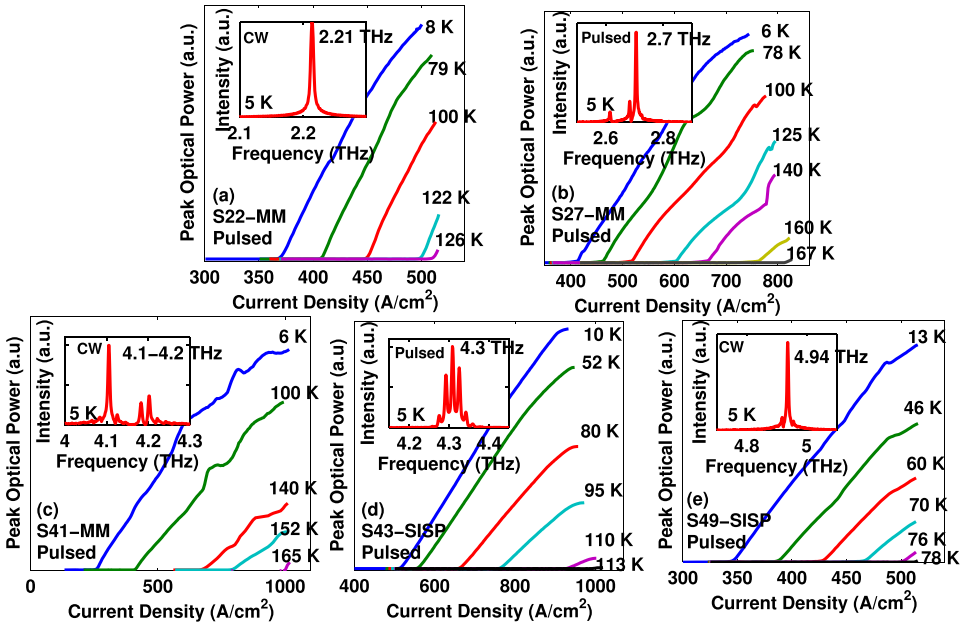

FIG. 3. Pulsed light-current measurements and lasing spectra (both pulsed and CW at ~5 K, insets) of the samples listed in Table I. (a) Sample S22-MM, (b) sample S27-MM, (c) sample S41-MM, (d) sample S43-SISP, and (e) sample S49-SISP.

TABLE II. Experimental parameters that were extracted from the measurements in Figures 3 and 4.

Name	Designed lasing energy [meV]	Measured lasing frequencies [THz/(meV)]	Expected activation energy from the lasing spectra [meV]	Measured activation energy from L_{max}-T [meV]	T_0 [K]	Tmax [K]
S22-MM	9.9	2.2/(9.14)	27	28	49	126
S27-MM	12.9	2.7/(11.20)	25	26	57	169
S41-MM	19	4.1/(16.95)	19	19	36	165
S43-SISP	19	4.3/(17.80)	18	14	29	113
S49-SISP	20.2	4.9/(20.43)	15–16	11	26	78

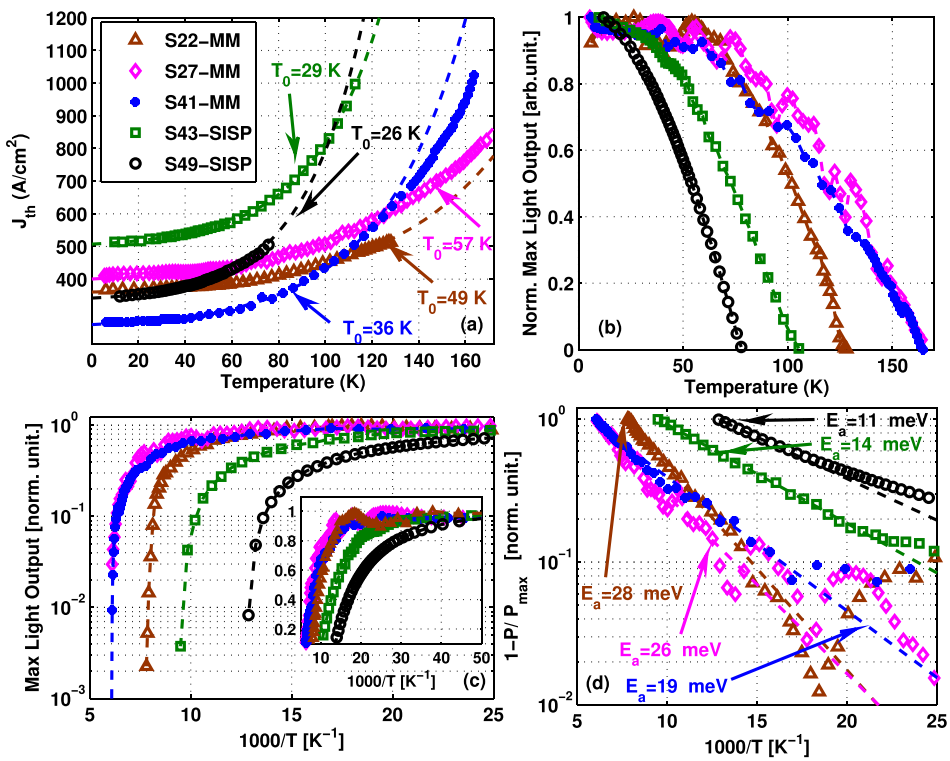

FIG. 4. (a) Threshold current densities vs. temperature and the associated parameter T_0, fitted by $J_{th} = J_1 + \exp(T/T_0)$. (b) The normalized output light intensity versus temperature in linear scale. (c) in semi-logarithmic scale versus the inverse temperature (Arrhenius plot); and (inset) zoom-in on the first decade. (d) The semi-logarithmic plot of $(1 - \frac{P_{out}(T)}{P_{out\,max}})$ with the fit (dashed lines) and activation energy values.

samples, supporting the activation energy model used in our analysis. Figure 4(d) also shows the expected deviation from the linear behavior at low temperatures. The fitted curves are linear down to about 50–80 K; this is in reasonable agreement with the expected electron heating from the simulation results shown in Figure 2(b).

Table II compares the activation energies extracted from Figure 4(d) to the values expected based on the measured lasing frequencies. The results are in good agreement, especially for MM devices which have higher T_{max}, so that there are more data points for fitting at the high-temperature end, supporting the presence of thermally activated LO phonon scattering. The activation energy values are much lower than the injector to extractor separation of $E_{42} \sim 36$ meV, which implies that thermal backfilling is not an important mechanism of performance degradation (in agreement with an earlier study[8]). For comparison, the threshold current parameters, T_0, extracted from Figure 4(a) are also listed in Table II. Although a high T_0 parameter is correlated with lower lasing energy, especially if extracted from the high temperature part of the curves, the interpretation is not as straightforward as the activation energy, which directly identifies the physical mechanism responsible for temperature degradation.

In conclusion, a method for investigating the dependence of lasing output power on temperature is presented. It is demonstrated to be a potentially useful characterization method for identifying mechanisms of temperature degradation, more so than the conventional methods of tracking threshold current density. Its validity is verified by applying it to a case study of vertical transition THz QCLs, where thermally activated LO phonon scattering is known to dominate the decrease of population inversion. Future work will apply this technique to other types of THz QCLs, notably diagonal transition THz QCLs.

The research was supported by NSF and Israel MoD, and A.A. was partially supported by the MIT-Technion and the Andrew and Erna Finci Viterbi Fellowships. The authors would like to thank Benjamin S. Williams and Sushil Kumar for their original measurements used in this work, Chun Wang I. Chan for fruitful discussions and advice, and John L. Reno for the MBE growths.

[1]G. P. Agrawal and N. K. Dutta, *Long-Wavelength Semiconductor Laser* (Van Nostrand Reinhold Company Inc., Canada, 1986).
[2]C. W. Ivan Chan, "Towards room-temperature terahertz quantum cascade lasers: Directions and design," Ph.D Thesis, Massachusetts Institute of Technology, Department of Electrical Engineering and Computer Science (2015).
[3]U. S. Fathololoumi, E. Dupont, C. W. I. Chan, Z. R. Wasilewski, S. R. Laframboise, D. Ban, A. Matyas, C. Jirauschek, Q. Hu, and H. C. Liu, Opt. Express **20**(4), 3866 (2012).
[4]B. S. Williams, Nat. Photonics **1**, 517 (2007).
[5]M. A. Belkin, Member, Q. J. Wang, C. Pflugl, A. Belyanin, S. P. Khanna, A. G. Davies, E. H. Linfield, and F. Capasso, IEEE J. Sel. Top. Quantum Electron. **15**(3), 952 (2009).
[6]J. Faist, *Quantum Cascade Lasers* (Oxford University Press, Oxford, UK, 2013).
[7]S. Kumar, "Development of terahertz quantum-cascade lasers," Ph.D Thesis, Massachusetts Institute of Technology, Department of Electrical Engineering and Computer Science (2007), available at http://hdl.handle.net/1721.1/40501.
[8]B. S. Williams, S. Kumar, Q. Qin, Q. Hu, and J. L. Reno, Appl. Phys. Lett. **88**, 261101 (2006).